Journal of Innovative Optical Health Sciences
Vol. 5, No. 2 (2012) 1250005 (9 pages)
© World Scientific Publishing Company
DOI: 10.1142/S1793545812500058

J. Innov. Opt. Health Sci. 2012.05. Downloaded from www.worldscientific.com
by HUAZHONG UNIVERSITY OF SCIENCE AND TECHNOLOGY on 10/24/18. Re-use and distribution is strictly not permitted, except for Open Access articles.

REAL-TIME OPTICAL MONITORING OF CAPILLARY GRID SPATIAL PATTERN IN EPITHELIUM BY SPATIALLY RESOLVED DIFFUSE REFLECTANCE PROBE

GUENNADI SAIKO* and ALEXANDRE DOUPLIK*,†,‡,§
*Department of Physics, Ryerson University
Toronto, ON M5B 2K3, Canada
†Clinical Photonics Lab, School of Advanced Optical Technologies (SAOT)
Friedrich-Alexander Erlangen-Nuremberg University
Erlangen, Germany
‡Medical Photonics Engineering Group
Chair of Photonics Technologies
Friedrich-Alexander Erlangen-Nuremberg University
Erlangen, Germany
§douplik@ryerson.ca

Accepted 14 January 2011
Published 16 March 2012

We developed a novel method for real-time monitoring of alteration of the local epithelium vessel/capillary and blood oxygenation spatial pattern in epithelium exploiting a compact fibre sensor system based on spatially and spectrally resolved diffuse reflectance. The method is based on collection of spatially resolved diffuse reflectance $R(\lambda)$ by fiber sensors. The spatial resolution is provided as a dependence of $R(\lambda)$ on a set of distances ρ between the source and detector (attenuation curve). It is expected that the new method can reasonably extract the minor spatial deviations of oxygenation and local blood volume fraction — parameters, directly related to the local vessel density and capillary spatial patterns in the epithelium. Light scattering in visible range is naturally taken into account in the proposed method.

Keywords: Spatially resolved diffuse reflectance; fiber optics; biospectroscopy; diagnostics; shock; cancer.

1. Introduction

Monitoring the epithelium vessel/capillary microcirculation spatial pattern is critically important for preventing rapidly developing life-threatening syndromes such as shock or systemic organ failures.[1] Shock can have a variety of effects, but all relate to problems with the body's circulatory system. The ultimate outcome of all kinds of shock is a dramatic decrease in blood pressure and blood volume.[1,2] Due to the drop in the blood pressure and blood perfusion, a local hypoxia is developed, and the blood vessel/capillary network eventually collapses.[1]

J. Innov. Opt. Health Sci. 2012.05. Downloaded from www.worldscientific.com
by HUAZHONG UNIVERSITY OF SCIENCE AND TECHNOLOGY on 10/24/18. Re-use and distribution is strictly not permitted, except for Open Access articles.

Shock development propagates from the small vessels that are closer to the surface, toward the magisterial arteries and heart, developing systemic hypoxia, and eventually metabolism breakdown and critical organ failure. During the period between the beginning of CVN spatial pattern alteration and development of system hypoxia chances to recover the patient out from the shock drop dramatically from 15%−25% to 75%−85% in terms of the mortality rate.[1,2] The time scale of these processes to spin off from the local capillary loops pattern alteration up to a system organ failure varies from 10−15 min up to 1−2 h, depending on a particular type of shock and medical conditions. Another important application field for the capillary spatial pattern monitoring is cancer diagnostics. Spatial arrangement of the blood vessels within the cancer lesion is irregular and in general denser than that of in healthy or benign tissue due to cancer angiogenesis.[3] Thus, an analysis of spatial distribution of blood vessels can be supplementary to other methods of cancer detection, e.g., redox scanning[4] and multiphoton microscopy.[5]

The main goal of the current work is to develop a technique, which provides monitoring of the CVN spatial pattern relative peculiarities temporally or spatially for consequently shock or cancer diagnostics.

To date, a variety of optical techniques is widely used for noninvasive or minimally invasive medical diagnostics and real-time monitoring of shock development or cancer diagnostics. With the notable exception of Doppler ultrasound[6] and laser Doppler flowmetry,[7] most of these techniques are different modalities of diffuse reflectance spectroscopy, a clinically proven optical technique for *in vivo* medical diagnostics. In particular, pulse oxymetry,[2] near-infrared (NIRS),[8] time[9] and frequency[10] domain spectroscopy are currently exploited for clinical measurement of blood perfusion *in vivo* using blue, green and near-infrared (NIR) wavelength ranges. The disadvantage of the existing methods is a too low spatial resolution to resolve the capillary loop pattern spatial arrangements and/or high dependence on scattering contribution that may lead to severe inaccuracies in estimation of the spatial pattern of the local microcirculation. The current spatial resolution is marginal as the periodic size of fine capillary density pattern normally is an order of 100−200 μm according to the molecular oxygen diffusion length within the biological tissues. The Doppler Spectral Optical Coherence Tomography (DOCT) can provide an adequate spatial resolution[11] to estimate the capillary density pattern; however, this method is still relatively complex, bulky and expensive for routine use in clinics particularly in Intensive Care Units (ICUs).

In the present work, we propose a method to overcome the above-mentioned limitations. The method is based on measuring a dependence of the diffuse reflectance (R) on the distance ρ between the source and detector — the attenuation curve. As the signal on the detector is conditioned mainly by the light absorption and scattering within the path between the light source and detector, the measured signal should be sensitive to tissue heterogeneities, namely variations of spatial distribution of blood due to the major blood vessels and capillary grid, which is expected to manifest itself in spatially resolved diffuse reflectance measurements.

The method extends applicability of diffuse reflectance techniques to detection of optical inhomogeneities on depth comparable with $l'_s = \frac{1}{\mu'_s}$, which is in the range of 100−300 μm for most biological surface tissues in visible range of spectrum.[12,13] Blood vessels can be found at this depth in epithelium and mucosa.[12]

The article is structured as: first, identifying relevant histological and physical model of tissue; second, quantifying effects of inhomogeneities on the diffuse reflectance and estimating their detectability; third, testing the method using numerical simulations, and finally, discussing the results, applicability and limitations of the method.

2. Skin Tissue Model

2.1. *Morphology*

The skin tissue is roughly divided into three main layers: the epidermis, dermis, and subcutaneous fat layer. However, from morphological point of view, the structure is much more complex and may include up to seven[14] or nine[15] distinct layers. Further discussion will be based on optical parameters and thicknesses derived from the seven-layer model[14] (Table 1).

The capillaries extend from the arteriole and venule in the subcutaneous tissue into the dermis and form two blood vessel layers: a deep blood net dermis (or cutaneous plexus) in the lower part of

J. Innov. Opt. Health Sci. 2012.05. Downloaded from www.worldscientific.com
by HUAZHONG UNIVERSITY OF SCIENCE AND TECHNOLOGY on 10/24/18. Re-use and distribution is strictly not permitted, except for Open Access articles.

Table 1. Optical parameters of skin tissue based on the seven-layer model of Meglinski and Matcher[14] at 633 nm.

Layer	μ_a (mm^{-1})	μ_s' (mm^{-1})	Thickness, d (mm)
Stratum corneum	0.00586	14	0.02
Living epidermis	0.00482	9	0.08−0.1
Papillary dermis	0.03341	3	0.15−0.2
Upper blood net dermis	0.2413	1.75	0.08−0.1
Reticular dermis	0.03341	5	1.4−1.6
Deep blood net dermis	0.08078	1.5	0.08−0.12
Subcutaneous fat	0.04127	1.25	6−6.5

the dermis (reticulation network) and an upper blood net dermis (or subpapillary plexus) in the upper part of the dermis (vascular network). Loops of small capillaries from subpapillary plexus ascend to papillary dermis, with small vessels lying close to epidermal basement membrane.

Based on this model, we can assess homogeneity of each layer on the scale of typical $l_s' = \frac{1}{\mu_s'}$ (100 μm). The epidermis (approximately 100 μm thick) does not have significant optical inhomogeneities on this scale and can be considered as a homogeneous layer. Papillary dermis and subpapillary dermis (approximately 200 μm thick) consist of homogeneous tissue with periodic capillaries (100−200 μm apart). Similar to blood in capillaries, which demonstrates significant absorption in visual range of spectrum, we can emulate this layer as a homogeneous layer with perturbations.

The underlying layer, upper blood net dermis (subpapillary plexus, 80−100 μm thick), contains a dense vascular network of blood vessels and can be considered as a homogeneous layer as well.

The next layer, reticular dermis (1.4−1.6 mm thick), is a homogeneous tissue with inclusion of capillaries, which can be considered as perturbations as well.

Thus, to monitor blood capillaries, we can monitor either capillaries protruding through papillary dermis and subpapillary dermis or upper blood net dermis. Capillaries in reticular dermis are optically shielded by subpapillary plexus and least likely will be able to manifest themselves on spatially resolved measurements.

2.2. *Lattice model*

Based on the previous discussion, we can consider the bio-tissue as homogeneous medium, and the variations of blood spatial distribution as local heterogeneities of optical parameters.

In radiation transport theory, the diffuse reflectance from bio-tissues in geometries with significant source to detector distance $\rho(\rho \gg l_s' = \frac{1}{\mu_s'})$ can be described by two parameters: the coefficient of light absorption $\mu_a(\lambda)$ and the reduced coefficient of scattering $\mu_s'(\lambda)$.

Despite the light propagated through the tissue averages information about the local optical properties, these properties can be estimated at the light entry and exit points. This can be demonstrated using a following lattice model. If we consider the photon propagation inside the tissue as a random walk on a cubic lattice (Fig. 1) with a step size $l_s' = \frac{1}{\mu_s'}$,which is the photon travel distance long enough to "forget" the photon's original direction. Because the scattering becomes isotropic, and then the next photon move can be completely arbitrary — random walk) with $z = 0$ as a border ($z > 0$ corresponds to the interior). The photons are considered to be injected at a single point with coordinates (0,0,0) and collected at some other surface point $(x, y, 0)$. The light has only one path

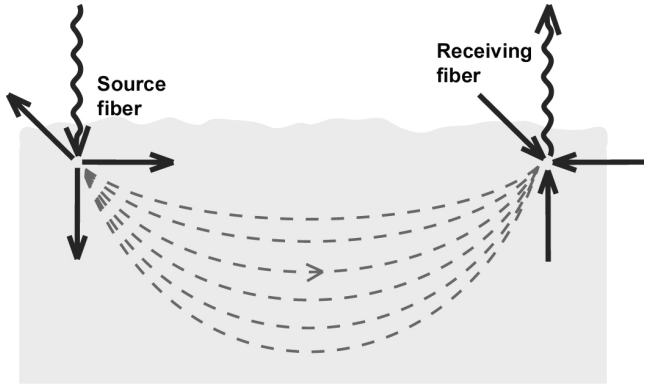

Fig. 1. Light propagation as random walk on a cubic lattice. The size of the lattice is $l_s' = \frac{1}{\mu_s'}$.

J. Innov. Opt. Health Sci. 2012.05. Downloaded from www.worldscientific.com
by HUAZHONG UNIVERSITY OF SCIENCE AND TECHNOLOGY on 10/24/18. Re-use and distribution is strictly not permitted, except for Open Access articles.

to enter the tissue ($(0,0,0)->(0,0,1)$) and exit the tissue ($(x,y,1)->(x,y,0)$) but numerous paths between the nodes $(0,0,1)$ and $(x,y,1)$. Thus, light propagation between the nodes $(0,0,1)$ and $(x,y,1)$ "averages" optical properties of the tissue, while the entry and exit bring data of the local optical properties in the vicinity of the source and receiving fiber. We can evaluate the impact of these local optical parameter variations using the path-length probability function.[16] For a homogeneous tissue attenuation can be calculated as

$$I/I_0 = \sum_l P_{x,y,0|0,0,0}(l) \exp\left(-\frac{\mu_a}{\mu_s'} l\right), \qquad (1)$$

where l is the photon path-length (in l_s' units) through the tissue between the delivering and receiving fibers and dimensionless $P_{x,y,0|0,0,0}(l)$ is the probability of the photon path with length l between the points (0,0,0) and $(x,y,0)$ at the absence of light absorption. Taking into account that

$$\begin{aligned} P_{x,y,0|0,0,0}(l) &= P_{0,0,1|0,0,0}(1) \times P_{x,y,1|0,0,1}(l-2) \\ &\quad \times P_{x,y,0|x,y,1}(1) \\ &= P_{x,y,1|0,0,1}(l-2), \end{aligned} \qquad (2)$$

then the Eq. (1) can be easily modified to include the local optical properties heterogeneities near the entry and exit points

$$\begin{aligned} I/I_0 &= \exp\left(-\frac{\mu_{a,s}}{\mu_s'}\right) \times \sum_l P_{x,y,1|0,0,1}(l-2) \\ &\quad \times \exp\left(-\frac{\mu_a}{\mu_s'}(l-2)\right) \\ &\quad \times \exp\left(-\frac{\mu_{a,f}}{\mu_s'}\right). \end{aligned} \qquad (3)$$

Here $\mu_{a,s}$ and $\mu_{a,f}$ are the local absorption coefficients in the vicinity of the light source and receiving fibres, respectively. By applying Eq. (2) again (in reverse order), Eq. (3) can be rewritten to bring the second term to the standard view (Eq. (1))

$$\begin{aligned} I/I_0 &= \exp\left(\frac{\mu_a}{\mu_s'} - \frac{\mu_{a,s}}{\mu_s'}\right) \times \sum_l P_{x,y,0|0,0,0}(l) \\ &\quad \times \exp\left(-\frac{\mu_a}{\mu_s'} l\right) \\ &\quad \times \exp\left(\frac{\mu_a}{\mu_s'} - \frac{\mu_{a,f}}{\mu_s'}\right). \end{aligned} \qquad (4)$$

The second term is the main (bulk) contributor, while the first and third terms reflect the local attenuation peculiarities in the vicinity of the source and the receiving fiber. Thus, if we keep either the source or the probe at a fixed location, for instance fixing the detector, and move the other end (e.g., the light source end), then the measured intensity will deviate from the average attenuation curve mainly due to pecularities of the light absorption in the vicinity of this moving end.

3. Numerical Verification

We have verified theoretical predictions using Diffision & Perturbation® simulation software[17] for numerical simulation of diffuse reflectance in tissue with perturbation. Blood capillaries were modeled by a spatial inhomogeneity (perturbation). The software package emulates the inhomogeneity by $1\,\mathrm{mm}^3$ defect with $\Delta\mu_a$ or ΔD equal to $1\,\mathrm{mm}^{-1}$ (here $\Delta D = -\Delta\mu_s'/(3\mu_s'^2)$). Thus, to emulate a tissue properly all dimensions, μ_a, and μ_s' should be scaled accordingly.

Based on $100-200\,\mu$m distance between capillaries and according to the Nyquist–Shannon sampling theorem,[18] we have to use not bigger than $50\,\mu$m optic fibers to detect an inhomogeneity of $100\,\mu$m and up, which is morphologically feasible. Thus, the reflectance signal was simulated on a grid with side $50\,\mu$m emulating $50\,\mu$m optical fibers. Scaling factor f, $f = 20$ was used consistently through our simulations: $\mu_a \to \mu_a/f$, $\mu_s' \to \mu_s'/f$, $L \to Lf$, where L is a distance (intercapillary distance, interfiber distance, layer depth, etc.).

Based on this scaling, the capillary was modeled by an inhomogeneity with $\Delta\mu_a = 20\,\mathrm{mm}^{-1}$, which is reasonable for visual range of spectrum (volume fraction of blood was estimated[9] to be in the range 0.01–0.3 for different layers of dermis). Reduced scattering coefficient and absorption coefficient of homogeneous tissue were set to $10\,\mathrm{mm}^{-1}$ and $0.1\,\mathrm{mm}^{-1}$, respectively.

We run two sets of simulations. First, we simulated a relative change in reflectance signal on 1×1 mm plane if an inhomogeneity is placed on a different depth in the center of the sampling area (under the tenth fiber). Second, we simulated the relative change in reflectance signal on each of 20 fibers for different positions of inhomogeneity (both vertically and horizontally).

J. Innov. Opt. Health Sci. 2012.05. Downloaded from www.worldscientific.com
by HUAZHONG UNIVERSITY OF SCIENCE AND TECHNOLOGY on 10/24/18. Re-use and distribution is strictly not permitted, except for Open Access articles.

4. Results

In the first set of simulations, we placed an inhomogeneity on a different depth under the tenth fiber: 50, 100, 200, 300, and 400 μm (or 0.5, 1, 2, 3, and 4 in l'_s units). The intensity maps for 50, 100, 200, and 400 μm depth are depicted in Fig. 2. It is easy to see, that in case of inhomogeneity of 50−100 μm (or 0.5−1 in l'_s units) deep, its impact is localized and consequently sensed mostly by the closest fibers (1−2 fibers, see Figs. 2(a) and 2(b)). For 200−400 μm, we see a completely different behavior. Heterogeneity impact is not localized and now it can be sampled by all the fibers located in the vicinity of the inhomogeneity (see Figs. 2(c) and 2(d)).

To refine this effect, we run the second set of simulations. During this run, we simulated the relative change in reflectance signal on each of 20 fibers for different positions of inhomogeneity (both vertically and horizontally). Inhomogeneity was placed on the depth $z_i = 50 \times i$ μm (where i was an integer between 1 and 20) and under every other (odd) fiber.

In Figs. 3(a)−3(d), one can see the relative change in reflectance signal for inhomogeneity placed under 1st, 3rd, 7th, and 17th fibers on different depths. Here we plotted negative relative change in diffuse reflectance caused by absorption inhomogeneity (it is always negative for $\Delta\mu_a > 0$) vs. the position of the receiving fibre. We can see a change in the shape of curves, which occurred between inhomogeneity depth 2 and 3 (in l'_s units) — from localized (with a local maximum, which can be seen in Figs. 2(a) and 2(b)) for smaller depths to monotonic dependence, which is typical for bigger depths (Figs. 2(c) and 2(d)). It is also easy to see that only the homogeneities located at the depth which is not more than l'_s can be potentially identifiable by the proposed spatially resolved technique.

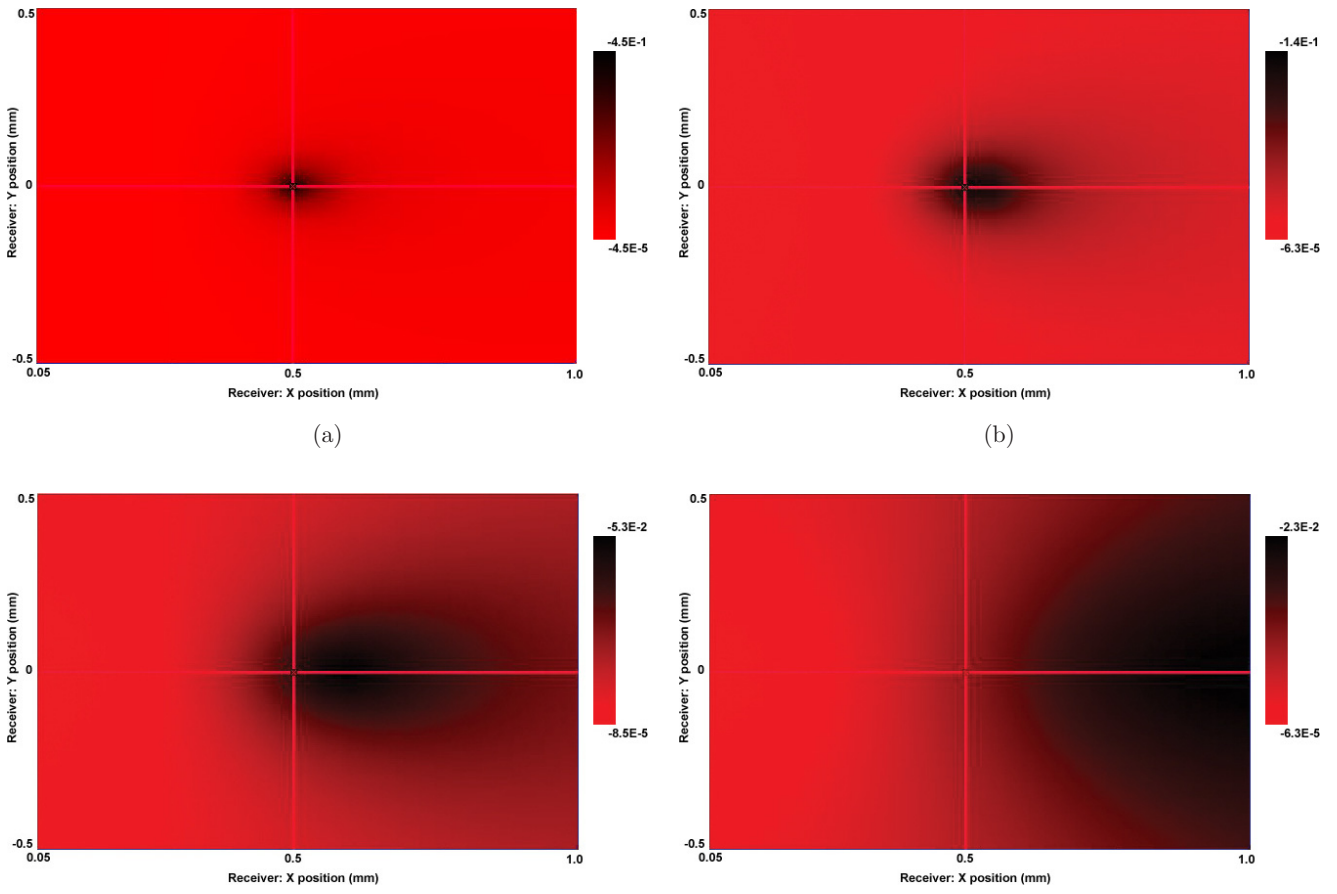

Fig. 2. Intensity maps for relative change in diffuse reflectance caused by absorption inhomogeneity placed under the 10th fiber (depicted by a cross) on the depth (a) 50, (b) 100, (c) 200, and (d) 400 μm.

J. Innov. Opt. Health Sci. 2012.05. Downloaded from www.worldscientific.com
by HUAZHONG UNIVERSITY OF SCIENCE AND TECHNOLOGY on 10/24/18. Re-use and distribution is strictly not permitted, except for Open Access articles.

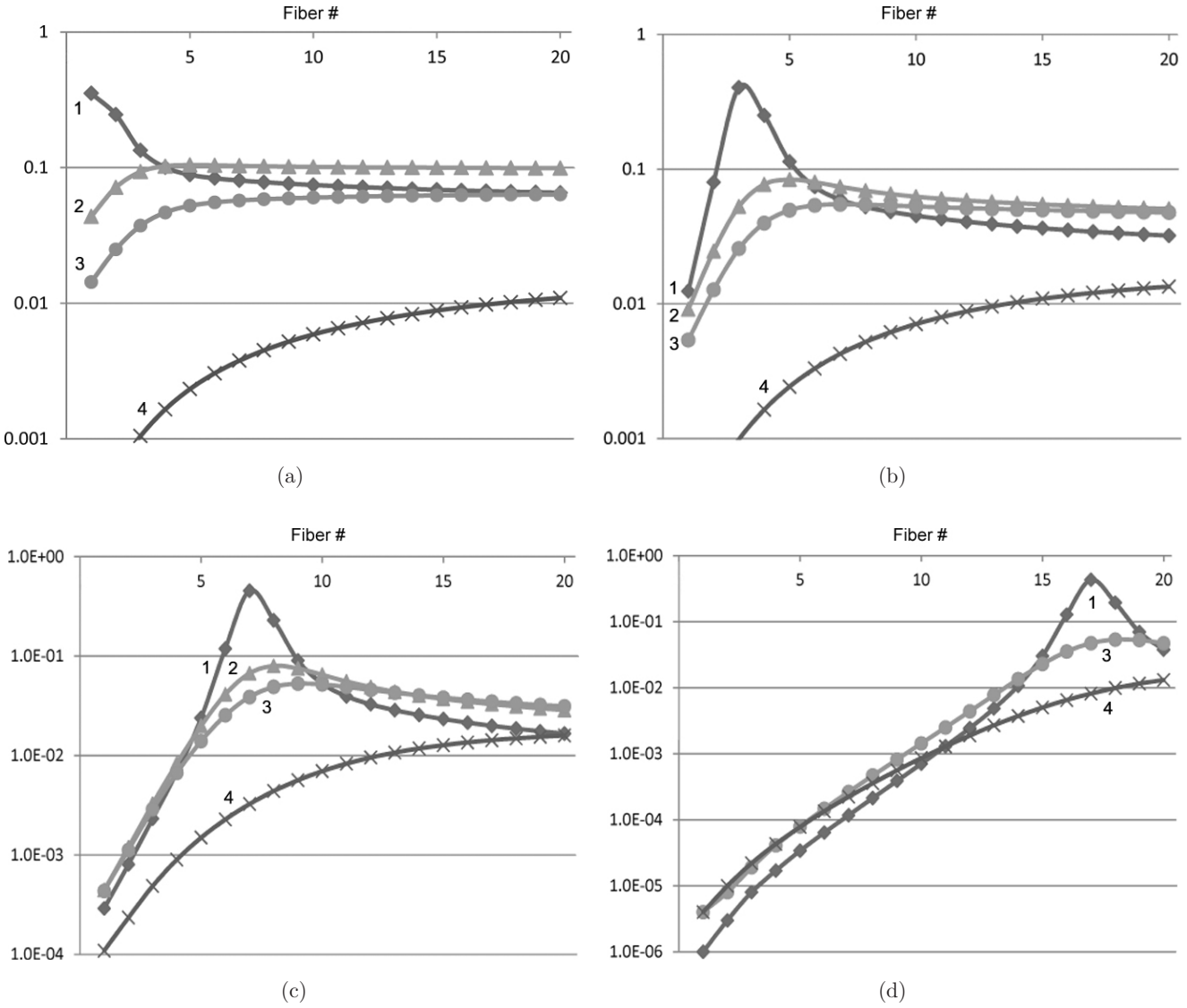

Fig. 3. The relative change in reflectance signal for inhomogeneity placed under (a) 1st, (b) 3rd, (c) 7th, and (d) 17th fibers on different depths. Curve 1 (♦) corresponds to 50 μm (0.5 l'_s) depth, curve 2 (▲) corresponds to 150 μm (1.5 l'_s) depth, curve 3 (•) corresponds to 200 μm (2 l'_s) depth, curve 4 (x) corresponds to 500 μm (5 l'_s) depth.

Finally, in Fig. 4, the superposition of relative changes in reflectance signal if homogeneities were placed under 5th, 9th, 13th, and 17th fiber simultaneously can be observed.

Initial background curve and convoluted signal for medium with inhomogeneities placed at $d = 0.5l'_s$ and $d = l'_s$ are presented in Fig. 4(a). In Fig. 4(b), we presented relative change in diffuse reflectance with respect to the original curve (homogeneous medium) for inhomogeneities placed at various depths.

Figures 4(a) and 4(b) show that the method is able to identify inhomogeneities located at the depth up to l'_s. It means that the method is applicable to a wide range of tissues, where top (bloodless) layer is thinner than l'_s (typically 100−200 μm), which can be true for mucosa and epithelium.

5. Discussion

Our numerical simulations confirmed our theoretical estimation, that the spatially resolved optical measurements are supposed to be sensitive to the optical inhomogeneities located within l'_s distance from the source or detector probe.

Illustrating this concept, the attenuation curve (Fig. 4(a)) contains two contributing parts. The background curve reflects contribution of both the

J. Innov. Opt. Health Sci. 2012.05. Downloaded from www.worldscientific.com
by HUAZHONG UNIVERSITY OF SCIENCE AND TECHNOLOGY on 10/24/18. Re-use and distribution is strictly not permitted, except for Open Access articles.

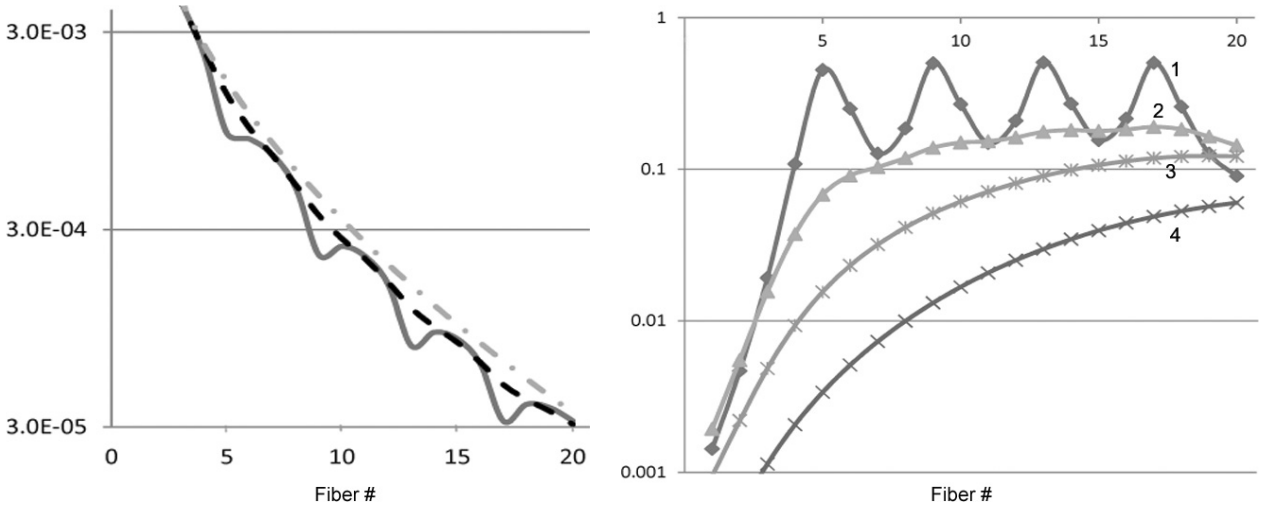

(a) (b)

Fig. 4. Algorithm of the capillary density estimation from attenuation curves. Simulations are based on the superposition of relative changes in reflectance signal if homogeneities were placed under 5th, 9th, 13th, and 17th fiber simultaneously. (a) Original attenuation curve measured. Dashed-dotted curve: background curve (no heterogeneities), solid curve corresponds defects on 50 μm (0.5 l'_s) depth, dashed curve corresponds defects on 100 μm (l'_s) depth. (b) Deconvolution of the attenuation curve. Curve 1 corresponds to 50 μm ($0.5l'_s$) depth, curve 2 corresponds to 150 μm ($1.5l'_s$) depth, curve 3 corresponds to 200 μm ($2l'_s$) depth, curve 4 corresponds to 500 μm (5 l'_s) depth.

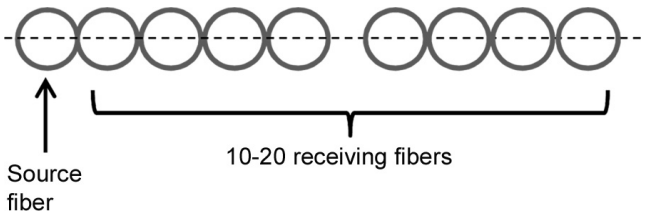

Fig. 5. The proposed design of the probe. One source fiber and 10−20 receiving fibers.

absorption and scattering integrated over the interrogation volume and linked to the second term of the Eq. (4). The second part (Fig. 4(b)) is a fine modulation of the attenuation curve due to the radiation transfer perturbation by local inhomogeneities on the scale l'_s and related to the first and third terms of the Eq. (4). On this scale, the capillary loops in papillary dermis are expected to be the major contributors.

To extract modulations, an experimental attenuation curve can be fitted with a proper fitting function (e.g., in diffuse approximation). Then, residuals of fitting correspond to fine modulations of the attenuation curve due to the radiation transfer perturbations. It should be pointed out that all estimations and numerical simulations above were performed in the diffuse approximation domain. The results should be similar in other ranges as well, but it requires experimental or Monte Carlo verification. Selection of a proper fitting function in these cases is less intuitive.

To increase the sensitivity, the method should be applied on tissues without thick epidermis layer, e.g., oral cavity epithelium. These tissues are characterized by both smaller capillary depth and lower scattering, which lead to smaller normalized capillary depth, and thus to increased sensitivity.

Even though the method is applicable to both visible and NIR range of spectrum, the use of the visible range will lead to detection of microcirculation alterations on earlier stages of shock and cancer development. The visible range is characterized by higher scattering and thus shorter "sensing distance" l'_s, comparable with capillary depth and intercapillary distance. Using NIR wavelengths will increase the "sensing depth" from

J. Innov. Opt. Health Sci. 2012.05. Downloaded from www.worldscientific.com
by HUAZHONG UNIVERSITY OF SCIENCE AND TECHNOLOGY on 10/24/18. Re-use and distribution is strictly not permitted, except for Open Access articles.

papillary dermis to upper blood net dermis, reticular dermis, and even deeper blood network, thus decreasing sensitivity to CVN alterations.

Various light paths may interrogate different numbers of capillary loops as well as different particular parts of the loops (e.g., venous or arterial). If we gradually change the distance between the source and probe, the calculated volume fractions will experience oscillations. The variations of the local RHb/HbO_2 volume fractions due to the different optical paths are expected to be the primary sources of these oscillations, at least as long as we stay in the diffuse approximation domain as mentioned above. Taking into account that blood oxygen saturation varies within the capillaries from 97%−99% (arterial blood) to 40%−60% (venous blood), the oxygenation is presumed to experience spatial oscillations as well.

The method can be implemented using laser diodes, which are virtually mixed together into one source. The diffuse reflectance can be captured using multiple fiber optode array with a step size of 50−100 μm. Based on our simulations, we can propose an array of optic fibers with 1 or 2 source fibers and 10−20 receiving fibers (see Fig. 5).

Multiple wavelengths can be used to extract additional information: volume fraction of oxy- and deoxy-hemoglobin, oxygenation, etc. Any change of RHb, HbO_2, and SO_2 and their spatial amplitudes will indicates physiological changes in microcirculation. This will be investigated in our future work.

Based on Eq. (4), we can expect that the proposed technique should be sensitive to spatial variations of the scattering coefficient. In addition to that, as we discussed earlier, the attenuation curve can be used to extract the scattering coefficient integrated over the interrogation volume. Such as some epithelial conditions and deseases (e.g., vitiligo[19]) are accompanied by change in the scattering coefficient, the proposed tool can be helpful for their quantitative diagnostics or treatment evaluation.

It should be pointed out that while the numerical simulations demonstrated detectability of capillaries in tissues, interpretation of real-life measurements can be complicated due to irregularities of inhomogeneity spatial distribution in tissues. Further studies, including Monte Carlo simulations, experiments on phantom and biological tissues are required to develop a clinic-ready diagnostic technique.

In conclusion, we described the theoretical base and numerical proof of concept for detection of spatial pattern of capillary grid exploiting a compact fibre sensor system based on spatially resolved diffuse reflectance.

Acknowledgments

The authors gratefully acknowledge funding of the Erlangen Graduate School in Advanced Optical Technologies (SAOT) by the German National Science Foundation (DFG) in the framework of the excellence initiative for support of this study.

References

1. P. A. van Beest, J. J. Hofstra, M. J. Schultz, E. C. Boerma, P. E. Spronk, M. A. Kuiper, "The incidence of low venous oxygen saturation on admission to the intensive care unit: A multi-center observational study in The Netherlands," *Critical Care* **12** (12), R33 (2008).
2. W. C. Shoemaker, C. C. Wo, S. Yu, F. Farjam, D. Thangathurai, "Invasive and noninvasive haemodynamic monitoring of acutely ill sepsis and septic shock patients in the emergency department," *Eur. J. Emerg Med.* **7**, 169−175 (2000).
3. Angiogenesis, National Cancer Institute, U.S. National Institutes of Health, Bethesda, Maryland, USA. Available at http://www.cancer.gov/cancertopics/understandingcancer/angiogenesis (2005−2011).
4. H. N. Xu, B. Wu, S. Nioka, B. Chance, L. Z. Li, "Quantitative redox scanning of tissue samples using a calibration procedure," *J. Innov. Opt. Health Sci.* **2**, 375−385 (2009).
5. X. Jiang, S. Zhuo, J. Chen, "Diagnostic application of multiphoton microscopy in epithelial tissues," *J. Innov. Opt. Health Sci.* **4**, 159−163 (2011).
6. B. Bein, P. Meybohm, E. Cavus, P. H. Tonner, M. Teinfath, J. Scholz, V. Doerges, "A comparison of transcranial Doppler with near infrared spectroscopy and indocyanine green during hemorrhagic shock: A prospective experimental study," *Critical Care* **10**(10), R18 (2006).
7. N. Skrebova Iekje, "Potential of *in vivo* latent-time estimation by laser and optical techniques in clinical and experimental dermatology," *J. Innov. Opt. Health Sci.* **4**, 421−428 (2011).
8. B. A. McKinley, R. G. Marvin, C. S. Cocanour, F. A. Moore, "Tissue hemoglobin O_2 saturation during resuscitation of traumatic shock monitored using near infrared spectrometry," *J. Trauma: Injury, Infection, Critical Care* **48**, 637−642 (2000).

J. Innov. Opt. Health Sci. 2012.05. Downloaded from www.worldscientific.com
by HUAZHONG UNIVERSITY OF SCIENCE AND TECHNOLOGY on 10/24/18. Re-use and distribution is strictly not permitted, except for Open Access articles.

9. T. H. Pham, R. Hornung, H. P. Ha, T. Burney, D. Serna, L. Powell, M. Brenner, B. J. Tromberg, "Noninvasive monitoring of hemodynamic stress using quantitative near-infrared frequency-domain photon migration spectroscopy," *J. Biomed. Opt.* **7**, 34−44 (2002).
10. R. A. De Blasi, S. Palmisani, D. Alampi, M. Mercieri, R. Romano, S. Collini, G. Pinto, "Microvascular dysfunction and skeletal muscle oxygenation assessed by phase-modulation near-infrared spectroscopy in patients with septic shock," *Intensive Care Med.* **31**, 1661−1668 (2005).
11. A. Douplik, D. Morofke, S. Chiu, V. Bouchelev, L. Mao, V. Yang, A. Vitkin, "In vivo real time monitoring of vasoconstriction and vasodilation by a combined diffuse reflectance spectroscopy and doppler optical coherence tomography approach," *Lasers Surg. Med.* **40**, 323−331 (2008).
12. J. Mobley, T. Vo-Dinh, Optical properties of tissue, Chap. 2, *Biomedical Photonics Handbook*, T. Vo-Dinh, Ed., pp. 1−75, CRC Press (2003).
13. A. N. Bashkatov, E. A. Genina, V. N. Tuchin, "Optical properties of skin, subcutaneous, and muscle tissues: A review," *J. Innov. Opt. Health Sci.* **4**, 9−38 (2011).
14. I. V. Meglinski, S. J. Matcher, "Quantitative assessment of skin layers absorption and skin reflectance spectra simulation in the visible and near-infrared spectral regions," *Physiol. Meas.* **23**, 741−753 (2002).
15. T. Maeda, N. Arakawa, M. Takahashi, Y. Aizu, "Monte Carlo simulation of spectral reflectance using a multilayered skin tissue model," *Optical Rev.* **17**, 223−229 (2010).
16. R. F. Bonner, R. Nossal, S. Havlin, G. H. Weiss, "Model for photon migration in turbid biological media," *J. Opt. Soc. Am. A* **4**, 423−432 (1987).
17. F. Martelli, S. Del Bianco, A. Ismaelli, G. Zaccanti, *Light Propogation through Biological Tissue and Other Diffusive Media*, SPIE Press (2010).
18. C. E. Shannon, "Communication in the presence of noise," *Proc. Institute of Radio Engineers* **37**, 10−21 (1949).
19. W. Gao, P. Lee, X. Zhang, "Characterization of vitiligo by *in vivo* scattering coefficient of human skin," *J. Innov. Opt. Health Sci.* **4**, 67−72 (2011).